PCCP

ARTICLE

Can the state of platinum species be unambiguously determined by the stretching frequency of adsorbed CO probe molecule?

Received 00th January 20xx,
Accepted 00th January 20xx

DOI: 10.1039/x0xx00000x

www.rsc.org/

Hristiyan A. Aleksandrov,[a,b] Konstantin M. Neyman,[b,c] Konstantin I. Hadjiivanov,[d] and Georgi N. Vayssilov[a*]

The paper addresses possible ambiguities in determination of the state of platinum species by the stretching frequency of a CO probe, which is a common technique for characterization of platinum-containing catalytic systems. We present a comprehensive comparison of the available experimental data with our theoretical modeling (density functional) results of pertinent systems – platinum surface, nanoparticles and clusters as well as reduced or oxidized platinum moieties on ceria support. Our results for CO adsorbed on-top on metallic Pt^0, with C-O vibrational frequencies in the region 2018-2077 cm^{-1}, suggest that a decrease of the coordination number of the platinum atom, to which CO is bound, by one lowers the CO frequency by about 7 cm^{-1}. This trend corroborates the Kappers-van der Maas correlation derived from analysis of experimental stretching frequency of CO adsorbed on platinum-containing samples on different supports. We also analyzed the effect of the charge of platinum species on the CO frequency. Based on the calculated vibrational frequencies of CO in various model systems, we concluded that the actual state of the platinum species may be mistaken based only on the measured value of the C-O vibrational frequency due to overlapping regions of frequencies corresponding to different types of species. In order to identify the actual state of platinum species one has to combine this powerful technique with other approaches.

Introduction

Transition metals are key components in various catalysts and one of the most widely used metals is Pt. It can be deposited as large particles exposing Pt(111) surface,[1] nanoparticles,[2,3] and smaller particles,[4] or even mononuclear Pt species.[5-8] The catalytic performance of the platinum-containing systems may be different depending on the platinum oxidation state, dispersion, location and, for metal particles, on the morphology.[9] Hence, it is crucial that all types of Pt catalytic sites are distinguished and characterized. One of the well-established techniques for characterization of such systems is adsorption of CO as an infrared (IR) probe molecule, where the change in the vibrational C-O frequencies is used for detecting different Pt sites in the catalytic system.[10] Among the factors that can influence the C-O vibrational frequency, when a CO probe molecule is adsorbed on platinum species, are: (1) adsorption mode of the CO, which for metallic platinum can be bound linearly to one Pt atom (on-top mode), to a Pt-Pt bond (bridge mode) or to the nearest three or four Pt atoms (hollow modes); (2) oxidation state and charge of the Pt adsorption center; (3) coordination number (CN) of Pt atoms on which the CO probe is adsorbed; (4) CO coverage. For deposited platinum systems an additional factor is the nature and redox state of the support. Recently, much attention has been paid to the Pt/CeO_2 systems, since the redox ability of ceria makes them efficient catalysts of various industrial processes, such as preferential CO oxidation,[11,12] water gas shift reaction,[13] conversion of automotive exhaust gases into harmless ones,[14,15] reforming of alcohols,[16] conversions in fuel cell catalysts,[17] etc. The catalytic role of ceria is commonly considered to be related to its reducibility at elevated temperature. When ceria is heated sufficiently, O_2 is desorbed, O vacancies are created in the material and each O vacancy leads to the reduction of two cations Ce^{4+} to Ce^{3+}. The process is reversible upon reactions with oxygen[18,19] or other oxidizing species.[20,21]

Numerous experimental studies of Pt/CeO_2 systems used IR spectroscopy of adsorbed CO for clarification of the state of platinum species (Table 1) and their catalytic performance.[4,22-30] For instance, Happel et al.[22] have detected in IR spectra several vibrational bands when CO was adsorbed on ceria supported platinum nanoparticles (Table 1). The bands at 1875 and 2080 cm^{-1} were attributed to CO in the bridge and top

[a] Faculty of Chemistry and Pharmacy, University of Sofia, 1126 Sofia, Bulgaria
e-mail: gnv@chem.uni-sofia.bg.
[b] Departament de Ciència de Materials i Química Física & Institut de Química Teòrica i Computacional, Universitat de Barcelona, 08028 Barcelona, Spain.
[c] Institució Catalana de Recerca i Estudis Avançats (ICREA), 08010 Barcelona, Spain
e-mail: konstantin.neyman@icrea.cat.
[d] Institute of General and Inorganic Chemistry, Bulgarian Academy of Sciences, Sofia 1113, Bulgaria.
* Corresponding author e-mail address: gnv@chem.uni-sofia.bg.

Electronic Supplementary Information (ESI) available: Information includes sketches of all modeled $Pt_8(CO)$ complexes in gas phase and some of their energetic and structural characteristics, structure of e-reg/$(CO)_2$ complex, and figure with the changes of the CO stretching frequency versus oxidation state and Bader charge of mononuclear platinum species. See DOI: 10.1039/x0xx00000x

positions, respectively, at Pt(111) facets, while the band at 2066 cm^{-1} was assigned to CO molecules adsorbed on the low coordinated platinum atoms at edges of the particles. Two other bands were also detected at 2053 and 2090-2100 cm^{-1}. The first one was associated with CO molecules located close to the interface between Pt nanoparticles and reduced ceria support. The second band was assigned to CO adsorbates in close proximity to O species located at the Pt nanoparticles. Similar two vibrational bands were found also by Bazin et al.,[4] at 2054 cm^{-1} and at 2096 and 2101 cm^{-1} (Table 1), when smaller Pt clusters were present in the investigated Pt/CeO_2 samples. The second band was again attributed to co-adsorption of CO and O on one Pt atom or two neighboring Pt atoms. However, the band at 2054 cm^{-1} was attributed to CO adsorbed on terrace sites. Other bands observed by Bazin et al.[4] were located at 2033, 2010 and 1937 cm^{-1}. The former two bands were attributed to CO adsorbed on low and very low coordinated Pt atoms belonging to small Pt clusters, while the origin of the last band remained unclear. It was proposed that it can be due to either bridge adsorption on Pt and Ce cations or adsorption on very low coordinated Pt sites. Ke et al.[23] investigated CO adsorption on PtO_x clusters supported on CeO_2. A band at 1833 cm^{-1} was assigned to bridge coordinated CO molecules on Pt (Table 1). Other bands were assigned to CO adsorbed on-top on Pt in different oxidation (charge) states: Pt^{2+} (2102-2120 cm^{-1}), $Pt^{\delta+}$ (2086-2092 cm^{-1}), Pt^0 (2066-2085 cm^{-1}).

In some of Pt/CeO_2 systems mononuclear Pt species were reported (no Pt-Pt bonds were detected).[31] Those Pt species were considered to be either ionic or neutral Pt atoms (in oxidation state zero). Daniel[24] assigned the bands at 2122 and 2128 cm^{-1} to CO on Pt^{2+} and Pt^{4+}, respectively. According to Qiao et al.[32] single Pt atoms uniformly dispersed on a FeO_x support can exist. On such samples a band at 2080 cm^{-1} was detected and assigned to on-top CO on monoatomic $Pt^{\delta+}$.

A comprehensive comparison of the available experimental results with theoretical modeling data for pertinent systems can help to clarify, which kind of catalytic Pt sites are present in the samples and to determine the origin of the detected bands. The key importance of such atomic-level understanding has been demonstrated in the recent experimental study by Ding et al.[9] Hence, in the present study we considered the adsorption of CO as a probe molecule on various platinum sites in a series of different models. We addressed two unsupported platinum species of different size: Pt_8 cluster and Pt_{79} nanoparticle (Fig. 1) in comparison with Pt(111) surface in order to ascertain how the coordination numbers of the involved in adsorption Pt atoms affect the binding energy of CO and the C-O vibrational frequency. The influence of ceria support on the adsorption characteristics of CO on Pt was also investigated. For that we employed models of Pt_8 cluster (Fig. 2 and 3) as well as neutral and cationic mononuclear Pt species (Fig. 4) anchored on a $Ce_{21}O_{42}$ nanoparticle.

In previous studies we have investigated computationally $Pt_8/Ce_{21}O_{42}$ system[33,34] along with various adsorption positions of PtO_x (x = 0-2) species on $Ce_{21}O_{42}$ nanoparticle.[8] In the latter work we identified the most stable mononuclear Pt species depending on the external conditions (O_2 partial pressure and temperature). In the present study we modeled interactions of all these platinum-ceria nanosystems with CO.

Computational method and models

The calculations are performed with a periodic density-functional method using a GGA exchange-correlation functional PW91,[35] as implemented in VASP code.[36-38] A plane-wave basis sets with a 415 eV cut-off for the kinetic energy and projector-augmented wave[38] description of core-valence electron interactions are employed.

Models with ceria support

An on-site Coulombic correction (U_{eff} = U-J)[39,40] is applied within the GGA+U scheme to 4f electrons on all Ce atoms to obtain their localized description in partially reduced Ce^{3+} ions. The U_{eff} value of 4.0 eV is used in line with previous studies.[5,8,33,34,41,42] Our model ceria particle $Ce_{21}O_{42}$ has diameter of about 1 nm.[43,44] A cubic 2.0 × 2.0 × 2.0 nm^3 unit cell is employed. In this way the nanoparticle $Ce_{21}O_{42}$ is separated from its periodically repeated images in the neighboring unit cells in the three Cartesian directions by at least 0.9 nm to minimize the spurious particle-particle interactions. Γ-point calculations are performed. Single-point total energy convergence tolerance at the self-consistency is set to 10^{-6} eV and structure optimizations continued until the maximum forces acting on each atom were less than 0.02 eV/Å. The reducibility of the Ce^{4+} ions has been accounted for by means of spin-polarized calculations.

The reported binding energies (BE) of the adsorbed CO on the Pt or Pt/ceria substrates are calculated as $BE(CO) = -E_{ad} - E_{sub} + E_{ad/sub}$, where E_{ad} is the total energy of the CO adsorbate in the gas phase, E_{sub} is the total energy of the corresponding platinum or Pt/ceria substrate system, and $E_{ad/sub}$ is the total energy of the substrate interacting with the CO adsorbate. With the above definition, negative values of BE imply favorable exothermic adsorption interaction.

Presented herein our calculated C-O vibrational frequencies ν are shifted by the difference of the harmonic frequency of the free CO calculated with the same computational approach ν_{calc}(CO-gas)=2129 cm^{-1} and the experimental anharmonic frequency of gas-phase CO, 2143 cm^{-1},

$\nu = \nu_{calc} - \nu_{calc}(CO\text{-}gas) + 2143$.

In this way the presented calculated values are increased by 14 cm^{-1} to be corrected for both the anharmonicity and the systematic error of the computational method. As it is commented below, this approach reproduces well (within 4 cm^{-1}) the experimental value for CO adsorption on regular Pt(111) surface.

Table 1. Summary of the experimental C-O vibrational frequencies (in cm^{-1}) for CO molecules adsorbed on Pt/CeO_2 and related systems.

Source	System	Frequency	Interpretation
Rupprechter et al.[57]	Pt(111) surface	2081	CO on-top at Pt(111) (low coverage)
	Pt(111) surface	2097	CO on-top at Pt(111) (high coverage)
Happel et al.[22]	Pt nanoparticles on ceria	1875	Bridge CO at regular Pt(111) facets
		2053	CO close to the interface between Pt nanoparticles and reduced ceria support
		2066	CO on low-coordinated Pt atoms at the particles edges
		2080	CO at regular Pt(111) nanofacets
		2090-2100	CO in close proximity to O species located at the Pt nanoparticles
Bazin et al.[4]	Pt clusters on ceria	1937	Unclear (bridge CO on Pt and Ce cations or adsorption on very low coordinated Pt sites)
		2010	CO on very small Pt particles (low-coordinated Pt atoms)
		2033	CO on low-coordinated Pt atoms of small Pt particles
		2054	CO on terrace sites
		2096 and 2101	Co-adsorption of CO and O on one Pt atom or two neighboring Pt atoms
Ke et al.[23]	PtO_x clusters on ceria	1833	Bridge CO on Pt
		2066-2085	CO on Pt^0
		2086-2092	CO on $Pt^{\delta+}$
		2102-2120	CO on Pt^{2+}
Jacobs et al.[25]	Pt/CeO_2	1975	CO on highly dispersed Pt
		2060	Linear Pt-CO on large Pt clusters
Jacobs et al.[27]	Pt/CeO_2	2030	Pt-CO on 2.3 nm platinum particles
Pillonel et al.[26]	Pt/CeO_2	2074 – 2054	Pt sites situated on different terraces
Holmgren et al.[28]	Pt/ceria	2030, 2001	CO on Pt (high dispersion of platinum)
		2067	CO on Pt
	Pt/ceria + Cl	2121	CO on Pt (partly oxidized)
Barrabe et al.[29]	Pt/CeO_2	2130-2120	CO on oxidized Pt or CO on Ce^{3+}
		2110	Unclear (appears on sample calcined at 900°C)
		2083	CO on Pt in less dense close packing arrangements - such as (100) faces
		2068	CO on Pt atoms in defect sites (steps and corners)
Jin et al.[30]	Pt particles on CeO_2	2084 to 2060	CO on Pt at terrace, step, and corner sites
		2091	CO adsorbed on Pt with an atom of oxygen at a neighboring site
		2131	CO coadsorbed with an oxygen atom on the same Pt atom
Daniel[24]	Pt/CeO_2	2096	CO adsorbed on single Pt atom on which O_2 is dissociatively adsorbed
	(Pt particle size of 30 nm)	2086	CO adsorbed on oxygen-free Pt (single Pt atom)
		2122	CO on Pt^{2+} sites
		2128	CO on Pt^{4+} sites

Please do not adjust margins

PCCP

ARTICLE

Models of mononuclear Pt species and Pt_8 cluster on $Ce_{21}O_{42}$

A platinum atom was considered anchored in different surface positions at the ceria nanoparticle.[8] We also added to these models one or two oxygen atoms (O_{add}) near the platinum atom in order to generate oxidized mononuclear platinum species, Pt^{2+} or Pt^{4+}, respectively. These structures mimic the deposition of neutral PtO or PtO_2 species on ceria. The formal charge of the platinum species and the number of Ce^{4+} cations reduced to Ce^{3+} are determined by the condition of the electro-neutrality of the whole system, which for the modeled types of species can be expressed in terms of atomic concentrations per nanoparticle as

$$[Ce^{3+}] + 2\times[O_{add}] - 2\times[O_{vac}] - 2\times[Pt^{2+}] - 4\times[Pt^{4+}] = 0, \quad (1)$$

where $[O_{vac}]$ and $[O_{add}]$ are the concentrations of the oxygen vacancies and added oxygen atoms, $[Pt^{2+}]$ and $[Pt^{4+}]$ are the concentrations of Pt^{2+} and Pt^{4+} ions, and $[Ce^{3+}]$ is the concentration of Ce^{3+} ions. Note that the balance in eq. (1) relies on the assumption that the added O atoms form O^{2-} ions in the system, while the equation should be modified if peroxo (O_2^{2-}) or superoxo (O_2^-) species[8] are formed. The equation is based on a simple balance of the number of electrons in the system and holds also for real neutral systems. All structures under scrutiny are denoted according to their sequence in Fig. 4 and the number of O vacancies or additional O centers (in the same way as the parent structures without adsorbed CO in Ref. 8). For example the labels c-1v/CO and c-2v/CO denote structures with one and two oxygen vacancies in the ceria nanoparticle and location of Pt species as shown in Fig. 4, series c. The notations d-1O/CO and d-2O/CO correspond to the structures with location of Pt species as in Fig. 4, series d, and one and two additional O centers in the model forming PtO or PtO_2 moiety, respectively. For comparison of the relative stability of different species we also calculated their relative energies, E_{rel}, with respect to the most stable structure for each stoichiometry.

The structures of the isolated model cluster Pt_8 used for deposition on the ceria nanoparticles and of the supported species $Pt_8O_x/Ce_{21}O_{42-x}$ (x = 0, 1) are presented elsewhere.[33,34,45]

Reference platinum systems - Pt(111), Pt_{79} nanoparticle and Pt_8 cluster.

Terrace sites on sufficiently large Pt particles of regular structure can be represented with the help of periodic slab models. To this end, single-crystal Pt(111) surface and {111} nanofacets of Pt particles were modeled by a five-layer slab with a $p(3\times3)$ surface unit cell. There, the three "top" atomic layers were allowed to relax, whereas the "bottom" two layers were fixed at the calculated for Pt bulk Pt-Pt distance of 282 pm.[46] The vacuum spacing between adjacent slabs was larger than 1 nm. All the calculations were carried out using a 5×5×1 Monkhorst-Pack k-point grid.[47]

The employed model nanoparticle Pt_{79} with the fcc structure has a truncated octahedral shape and exposes {111} facets together with very small {100} facets, consisting of 12 and 4 atoms, respectively. This particle has been positioned in a cubic cell with the lattice parameter a = 2 nm, which ensures vacuum spacing of ~1 nm between atoms in the neighboring periodically repeated cells. In order to explore in more detail the dependence of the C-O vibrational frequencies on the coordination number of Pt to which CO is bound, we also considered Pt_{69}, Pt_{51}, and Pt_{32} nanoparticles obtained by removing one, two and three layers, respectively, from a {111} facet of Pt_{79}. Calculations of the discrete particles have been performed at the Γ point in the reciprocal space.

The employed bare cluster Pt_8 has the structure g in Ref. 45, which was found to be the most stable among ten structures explored there.

Results

CO adsorption on unsupported platinum models

We modeled CO adsorption on unsupported platinum models of different sizes, starting with a small Pt_8 cluster, which changes notably its geometry upon CO adsorption. Next, we investigated CO adsorption on Pt_{79} nanoparticle and Pt(111) slab, where CO can be adsorbed on well-defined adsorption sites. The Pt(111) slab model is used to represent large Pt particles, where the corresponding regular terrace sites are in majority. The results obtained for these systems are summarized in Table 2 and several representative optimized structures are shown in Figure 1.

Table 2. Calculated energetic and structural characteristics of the adsorption complexes of one CO molecule with Pt_8, Pt_{79} and Pt(111) models as well as of one, seven and twelve CO molecules with $Pt_8O_X/Ce_{21}O_{42-Y}$ (X = 0 or 1, Y = 0, 1, or 4) models. Energy values are in eV, distances in pm, and vibrational frequencies in cm^{-1}.

	Ns[a]	#Ce[b]	BE[c]	CN[d]	r(Pt-C)	ν(C-O)[e]	Δr(C-O)[f]
Pt(111)/CO_on-top	0		-1.71	9	185	2077	1.4
Pt(111)/CO_bridge	0		-1.80	9-9	202, 203	1853	3.9
Pt_{79}/CO-terrace	0		-1.92	8	184	2065	1.6
Pt_{79}/CO-edge	0		-2.14	7	185	2045	1.8
Pt_{79}/CO-corner	0		-2.14	6	185	2041	1.9
Pt_8CO_a	2		-2.73	5	184	2041	2.2
Pt_8CO_b	2		-2.63	3	183	2024	2.4
$Pt_8CO/Ce_{21}O_{42}$_a	2	1	-2.84	5	183	2024	2.4
$Pt_8CO/Ce_{21}O_{42}$_b	2	1	-2.73	3	183	2011	2.6
$Pt_8CO/Ce_{21}O_{42}$_c	4	2	-2.58	6-2(2)	193, 209	1885	4.0
$Pt_8CO/Ce_{21}O_{42}$_d	2	1	-2.41	3	186	2012	2.4
$Pt_8CO/Ce_{21}O_{42}$_e	2	1	-2.33	5	184	2009	2.4
$Pt_8CO/Ce_{21}O_{42}$_f	4	2	-2.11	4-5	196, 210	1840	4.2
$Pt_8CO/Ce_{21}O_{42}$_g	2	1	-1.98	4	183	1997	2.9
$Pt_8CO/Ce_{21}O_{42}$_h	2	1	-1.75	3(1)	184	2021	2.3
$Pt_8O(CO)/Ce_{21}O_{42}$_a	4	4	-2.68	3(1)	183	2006	2.7
$Pt_8O(CO)/Ce_{21}O_{42}$_b	6	4	-2.25	3(1)	182	1958	3.5
$Pt_8O(CO)/Ce_{21}O_{42}$_c	6	4	-2.08	5	185	2023	2.2
$Pt_8(CO)_7/Ce_{21}O_{38}$	8	9	-2.06			[g]	
$Pt_8(CO)_{12}/Ce_{21}O_{38}$	8	8	-1.66			[h]	
$Pt_8(CO)_7/Ce_{21}O_{42}$	0	0	-2.11			[i]	
$Pt_8(CO)_{12}/Ce_{21}O_{42}$	0	0	-1.64			[j]	

[a] Number of unpaired electrons; [b] Number of Ce^{3+} cations [c] BE per CO adsorbate; [d] Coordination number of the Pt atom, on which CO molecule is adsorbed (number of contacts of the Pt atom with O atoms shown in parentheses); [e] Calculated frequencies are corrected by 14 cm^{-1} (see Section 2); [f] Elongation of C-O bond upon adsorption with respect to the calculated bond length in gas-phase CO of 114.2 pm; [g] On-top - 2050, 2033, 2021, 2008, 1999, 1998 cm^{-1}, bridge - 1784 cm^{-1}; [h] On-top - 2056, 2036, 2035, 2028, 2023, 2017, 1976 cm^{-1}, bridge - 1899, 1894, 1874, 1853, 1701 cm^{-1}; [i] On-top - 2057, 2035, 2025, 2017, 2009, 1959 cm^{-1}, bridge - 1836 cm^{-1}; [j] On-top - 2062, 2046, 2043, 2036, 2032, 2020, 1998 cm^{-1}, bridge - 1902, 1901, 1882, 1859, 1737 cm^{-1}.

We have modeled also 17 structures of the adsorption complex Pt_8CO using a cluster Pt_8,[45] where CO was adsorbed in various top, bridge and hollow positions (see Supporting Information). In the most stable structure Pt_8CO_a, BE(CO) = -2.73 eV, the coordination number (we assigned a cut-off 320 pm to calculate the CN) of the Pt atom to which the CO molecule is bound is 5 and the C-O vibrational frequency is 2041 cm^{-1}. Another structure Pt_8CO_b shows similar stability, BE(CO) = -2.63 eV, but lower coordination number of Pt, CN = 3, and lower C-O frequency, 2024 cm^{-1} (Table 2). As a trend, the C-O frequency increases with the coordination number of the Pt atom of Pt_8 accommodating on-top CO from 2018-2021 cm^{-1}, when the coordination number is 2, to 2037-2041 cm^{-1} when the coordination number reaches 4 and 5 (Table S1 of ESI).

CO is adsorbed in on-top (Pt(111)/CO_on-top) and bridge (Pt(111)/CO_bridge) positions of the regular Pt(111) model with BE(CO) -1.71 and -1.80 eV, respectively (Table 2). These values are lower than the BE(CO) values at Pt_8, since the Pt(111) surface exposes Pt atoms with CN = 9, which is significantly higher than the CN of the Pt atoms in Pt_8 cluster. The C-O vibrational frequency is 2077 and 1853 cm^{-1} at the on-top and bridge positions, respectively.

Three different on-top positions on Pt_{79} nanoparticle were studied: terrace, edge, and corner sites, where the coordination numbers of Pt atoms on which CO is adsorbed should be 9, 7, and 6, respectively. However, due to the large flexibility of the nanoparticle model one of the Pt-Pt distances becomes larger than 320 pm, when CO is adsorbed on terrace site, hence in this case we assigned CN = 8. This position is characterized by the lowest absolute value of BE(CO), -1.92 eV, while the adsorption complexes on the other two positions are by ~0.2 eV more stable. The C-O vibrational frequency for the terrace site is 2065 cm^{-1}. The ν(C-O) values for edge and corner sites are lower, 2045 and 2041 cm^{-1}, respectively (Table 2).

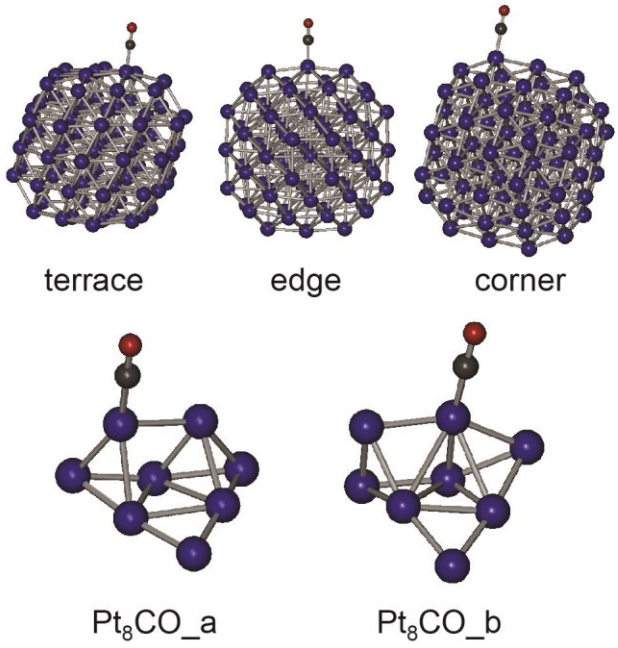

Figure 1
Optimized structures of the CO adsorbed on top positions at terrace, edge and corner sites on Pt_{79} nanoparticle. The two most stable Pt_8CO structures are also shown. Color coding: red – O; gray – C; dark blue – Pt. Cut-off for the Pt-Pt bonds is 330 pm.

CO adsorption on $Pt_8/Ce_{21}O_{42}$

Next, we studied CO adsorption on a Pt_8 cluster supported on ceria nanoparticle $Ce_{21}O_{42}$ (Fig. 2, Table 2). Previously we have found that Pt_8 cluster spontaneously donates one or two electrons to the ceria nanoparticles or (111) surface upon deposition there with concomitant formation of one or two Ce^{3+} ions.[33,34,42] We considered eight different adsorption complexes of one CO molecule on the $Pt_8/Ce_{21}O_{42}$ system: six complexes where CO interacts with one Pt atom at on-top position and two complexes where CO is adsorbed in a bridge position. The structures with on-top CO adsorption are most stable when the system has two unpaired electrons (one of which is on a Ce^{3+} cation). The structures with a bridge coordinated CO molecule are most stable with four unpaired electrons (of which two are on Ce^{3+} cations). Thus, adsorption of one CO molecule does not change the number of electrons transferred from Pt_8 to the $Ce_{21}O_{42}$ support. The most stable structure is $Pt_8CO/Ce_{21}O_{42}$_a with BE(CO) = -2.84 eV and CN(Pt) = 5 with respect to other Pt atoms. $Pt_8CO/Ce_{21}O_{42}$_b structure (with CN(Pt) = 3) is only by 0.11 eV less stable. In both cases CO is adsorbed on-top. The most stable structure with bridge adsorption of CO is $Pt_8CO/Ce_{21}O_{42}$_c characterized by BE(CO) = -2.58 eV. The C-O vibrational frequencies for the complexes with on-top CO coordination are in the range of 1997-2024 cm^{-1}. For the most stable two structures, $Pt_8CO/Ce_{21}O_{42}$_a and $Pt_8CO/Ce_{21}O_{42}$_b, the calculated frequencies are 2024 and 2011 cm^{-1}, respectively. When CO is adsorbed on bridge sites, $Pt_8CO/Ce_{21}O_{42}$_c and $Pt_8CO/Ce_{21}O_{42}$_f, the ν(C-O) values are 1885 and 1840 cm^{-1}, respectively. In accordance with the ν(C-O) values, the elongation of the C-O bond distances Δr(C-O) at bridge adsorption, 4.0-4.2 pm, exceeds that for the on-top adsorption, 2.3-2.9 pm (Table 2).

It was found that O spillover from ceria nanoparticles to Pt_8 cluster is exothermic by -0.1 ÷ -0.4 eV.[33,34] In the structures with O spillover the O atom is coordinated to two Pt atoms. Here we modeled O spillover from $Ce_{21}O_{42}$ nanoparticle to Pt_8 cluster for three structures with CO adsorbed on-top on different Pt atoms: in the structures $Pt_8O(CO)/Ce_{21}O_{42}$_a and $Pt_8O(CO)/Ce_{21}O_{42}$_b the CO molecule is co-adsorbed on one of the Pt atoms where O atom is also located, while in the structure $Pt_8O(CO)/Ce_{21}O_{42}$_c CO is adsorbed on a five-coordinated Pt atom, which is not connected to the O atom. In the most stable structure, $Pt_8O(CO)/Ce_{21}O_{42}$_a, BE(CO) = -2.68 eV is very similar to that in the corresponding structure without oxygen transfer, $Pt_8(CO)/Ce_{21}O_{42}$_b, BE(CO) = -2.73 eV. Hence, the O spillover does not change notably the binding energy of CO to the Pt_8 cluster. The C-O vibrational frequency in the $Pt_8O(CO)/Ce_{21}O_{42}$_a structure, 2006 cm^{-1}, also does not change notably compared to the value 2011 cm^{-1} in the structure without O spillover, $Pt_8(CO)/Ce_{21}O_{42}$_b. Each of the three considered structures features four Ce^{3+} cations. It means that O spillover leads to transfer of one additional electron from Pt_8 to $Ce_{21}O_{42}$ nanoparticle, since removing of an O atom from ceria generates two Ce^{3+} ions, while the analogous $Pt_8CO/Ce_{21}O_{42}$ structures before O transfer with an on-top adsorbed CO molecule contain one Ce^{3+} cation.

We also considered structures with 7 and 12 adsorbed CO molecules on the $Pt_8/Ce_{21}O_{42}$ model, $Pt_8(CO)_7/Ce_{21}O_{42}$ and $Pt_8(CO)_{12}/Ce_{21}O_{42}$ (Figure 3, Table 2). In $Pt_8(CO)_7/Ce_{21}O_{42}$ six of the CO ligands are coordinated on-top and one is bound at a bridge position. In $Pt_8(CO)_{12}/Ce_{21}O_{42}$ seven ligands feature on-top coordination and five are in bridge coordination. The average binding energy per CO ligand for the structure $Pt_8(CO)_7/Ce_{21}O_{42}$ is -2.11 eV, while for the structure $Pt_8(CO)_{12}/Ce_{21}O_{42}$ it is reduced to -1.64 eV. The C-O vibrational frequencies of the on-top CO molecules are in the regions 1959-2057 and 1998-2062 cm^{-1} for the structures with 7 and 12 CO molecules, respectively. For the bridged adsorbed CO molecules the corresponding frequency values are 1836 and 1737-1902 cm^{-1}. Both structures are calculated to be most stable as singlets without formation of any Ce^{3+} ions. It indicates that adsorption of several CO molecules induces reverse transfer of electrons from Ce^{3+} ions to the Pt_8 cluster.

In order to examine, whether reduction of the ceria support will affect the C-O vibrational frequencies and the number of unpaired electrons of the systems we modeled the above mentioned two systems with four O vacancies created in the ceria nanoparticle, structures $Pt_8(CO)_7/Ce_{21}O_{38}$ and $Pt_8(CO)_{12}/Ce_{21}O_{38}$ (Figure 3, Table 2).

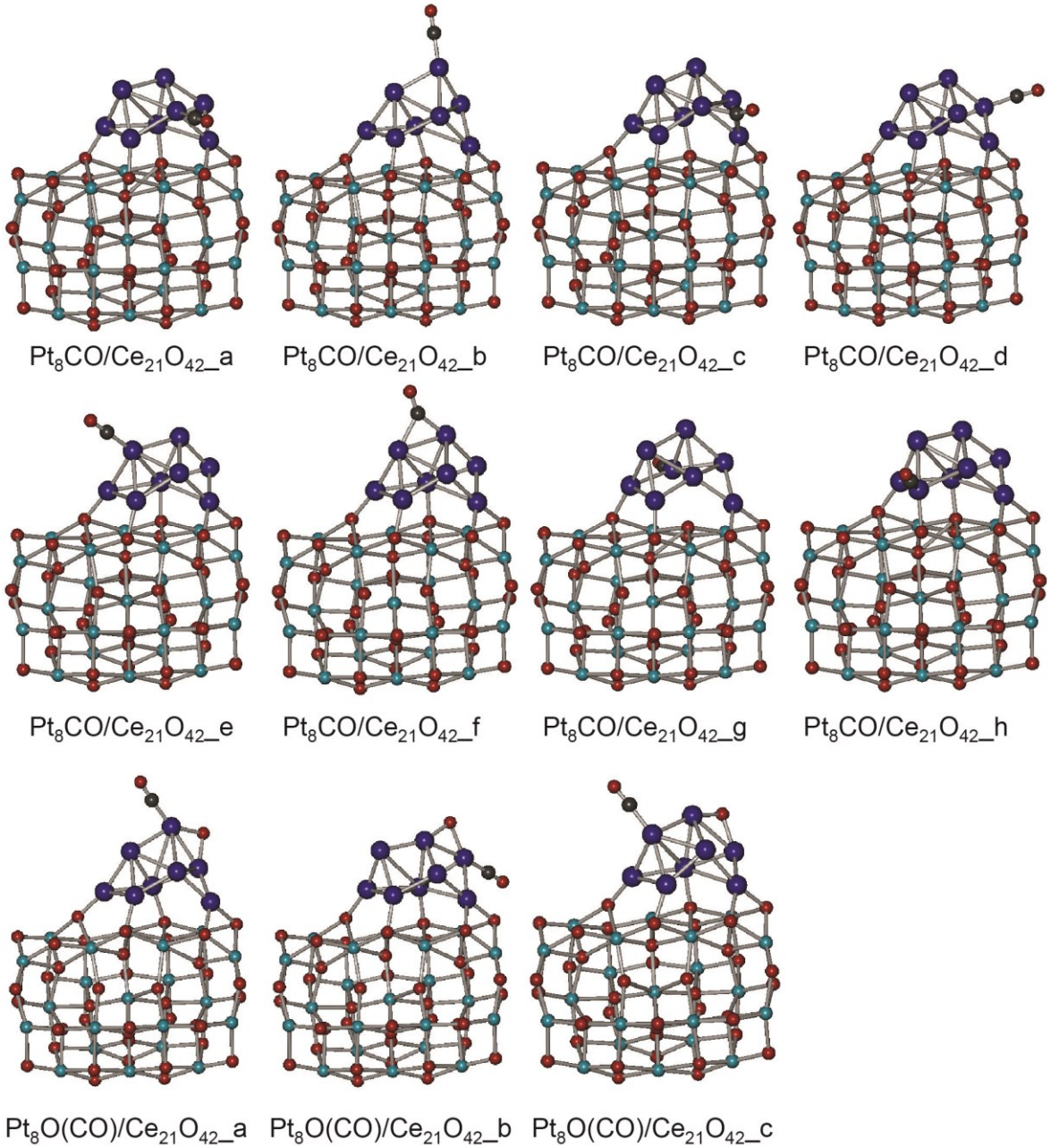

Figure 2
Optimized structures of the complexes $Pt_8(CO)/Ce_{21}O_{42}$ and $Pt_8O(CO)/Ce_{21}O_{41}$. Eight different positions were considered in the first case (a-h) and three in the second case (a-c). Color coding: red – O; gray – C; light blue – Ce; dark blue – Pt. Cut-off for the Ce-O and Pt-O bonds is 260 pm, while cut-off for the Pt-Pt bonds is 330 pm.

The oxygen atoms were removed from the positions found to be the most preferable ones for the bare $Ce_{21}O_{42}$ nanoparticle, i.e. low (two) coordinated O atoms.[43,44] The expected number of Ce^{3+} ions in the complexes should be ten - eight Ce^{3+} ions due to the four oxygen vacancies and two additional Ce^{3+} ions due to the transfer of the two electrons from Pt_8 cluster to the ceria nanoparticle. This is indeed the case for the pristine $Pt_8/Ce_{21}O_{38}$ structure or that with one adsorbed CO molecule. However, $Pt_8(CO)_7/Ce_{21}O_{38}$ and $Pt_8(CO)_{12}/Ce_{21}O_{38}$ structures are most stable with 8 unpaired electrons and there is a transfer of only one electron in the former structure and lack of transfer electrons from Pt cluster to the ceria support in the latter structure, when Pt clusters are covered by CO. This is in line with experimental results of Happel et al.[22] The creation of four O vacancies leads to only slight lowering of some of the C-O frequencies by 2-10 cm^{-1}. Solely the lowest frequencies of the on-top and bridged adsorbed CO are changed more significantly, by up to 39 and 52 cm^{-1}, respectively.

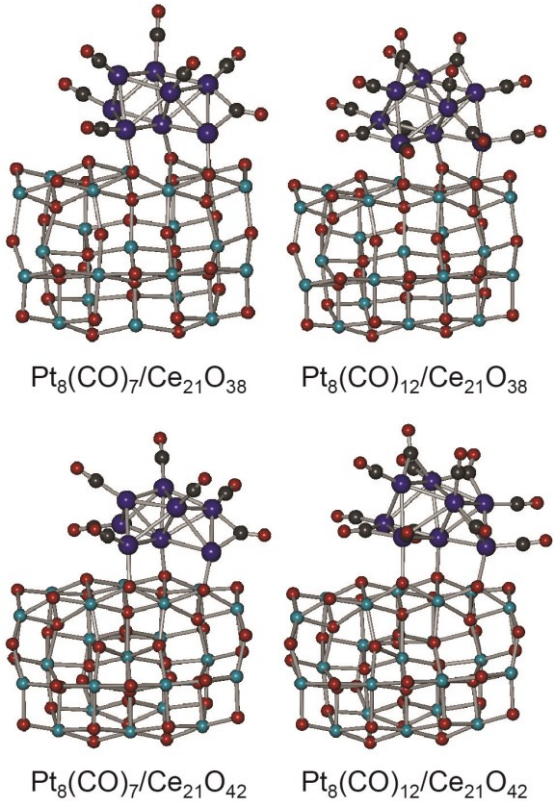

Figure 3
Optimized structures of the complexes with seven and twelve CO molecules adsorbed on regular $Pt_8/Ce_{21}O_{42}$ and reduced (containing four O vacancies) $Pt_8/Ce_{21}O_{38}$ structures. Color coding: red – O; gray – C; light blue – Ce; dark blue – Pt. Cut-off for the Ce-O and Pt-O bonds is 260 pm, while cut-off for the Pt-Pt bonds is 330 pm.

CO adsorption on mononuclear platinum species (PtO_X, X = 0-2) supported on ceria nanoparticle

Four positions of a single Pt atom on the (111) facets and on edges of $Ce_{21}O_{42}$ nanoparticle (denoted as a, b, c and d), where Pt is in oxidation state zero have been previously modeled by us.[8] Another structure, where Pt is on the small {100} facet (denoted as position e) features Pt in oxidation state +2 and two Ce^{3+} cations. The latter structure is more stable by 2.5-3.0 eV than the structures a-d. The structures a-e were modeled at different conditions – *i*) stoichiometric with $Pt/Ce_{21}O_{42}$ models; *ii*) oxidative with $PtO_X/Ce_{21}O_{42}$ (X = 1, 2) models; and *iii*) reductive with $Pt/Ce_{21}O_{42-Y}$ (Y = 1, 2) models. Oxidative conditions were simulated by adding one or two O atoms in the vicinity of Pt. Hence, PtO or PtO_2 species were formed, where the intended oxidation state of platinum is +2 or +4, respectively. Reductive conditions were simulated by creating one or two O vacancies in the ceria nanoparticle.

The modeled structures are shown on Figure 4 and the obtained results are summarized in Table 3. In all $PtCO/Ce_{21}O_{42-Y}$ (Y = 0 ÷ 2) structures linear O–Pt–C≡O complexes are formed, where PtCO moiety is coordinated to only one O center of the ceria nanoparticle. When CO is adsorbed on the oxidized platinum moieties in $PtO/Ce_{21}O_{42}$ and $PtO_2/Ce_{21}O_{42}$, the ligands around the Pt centers form triangular or square-planar complexes with the C atom of CO and two or three O centers.

The calculations reveal that CO is strongly bound to the atomic Pt^0 species of $Pt/Ce_{21}O_{42}$ a-d structures with BE(CO) exceeding -3.00 eV (in absolute value). Coordination of CO to the most stable structure $Pt/Ce_{21}O_{42}$-e is rather weak, BE(CO) = -0.17 eV, since there platinum species is Pt^{2+} and it is coordinated within a square of four O anions,[5,8] forming a coordination compound with the whole support particle serving as a polydentate ligand.[48] However, a more stable structure of this system, with BE(CO) = -0.62 eV, is formed when upon CO adsorption Pt^{2+} species is reduced to Pt^0 and moved out of its square-planar position. In this case, similar to the other complexes of CO with atomic Pt^0 species, a complex with linear O-Pt-C-O geometry is formed. This suggests that the interaction energy of CO with Pt^0 is sufficient to pull out Pt^{2+} species from their most stable square-planar position and force to facilitate its reduction to Pt^0.

The adsorption of the second CO molecule (in the structure e-reg/$(CO)_2$) further stabilizes the complex increasing the value of BE per CO molecule to -1.04 eV (Fig. S2). Concomitantly, the Pt species are re-oxidized to Pt^{2+}. The dicarbonyl complex is square planar and Pt^{2+} species interacts with two oxygen centers of ceria nanoparticle and carbon atoms of both CO molecules. In order to explore the influence of the ceria support we modeled a similar dicarbonyl complex on a larger $Ce_{40}O_{80}$ nanoparticle, where the BE per CO molecule is calculated to be 0.71 eV. Similar complexes of $Pt^{2+}(CO)_2$ were observed for CO adsorbed on platinum-containing zeolites.[49]

The BE(CO) values for CO adsorption on platinum species on reduced support $PtCO/Ce_{21}O_{42-Y}$ (Y = 1, 2) vary non-monotonically with respect to the values of the corresponding stoichiometric $PtCO/Ce_{21}O_{42}$ complexes as the maximal change in the BE(CO) value after reduction is 0.6 eV.

Addition of one or two oxygen atoms has significantly larger effect than reduction on the BE(CO) values due the oxidation of the platinum species to Pt^{2+} or Pt^{4+} cations. For the complexes with CO on Pt^{2+} the BE(CO) varies from -1.0 to -3.0 eV depending on the position of the platinum species on the ceria particle. Note that Pt^{2+} is present not only in the complexes $PtO(CO)/Ce_{21}O_{42}$, but also in two of the complexes with two additional oxygen atoms, $PtO_2(CO)/Ce_{21}O_{42}$, structures b and e, due to formation of peroxo species. The only complexes containing Pt^{4+} ion are those of series a, c, and d.

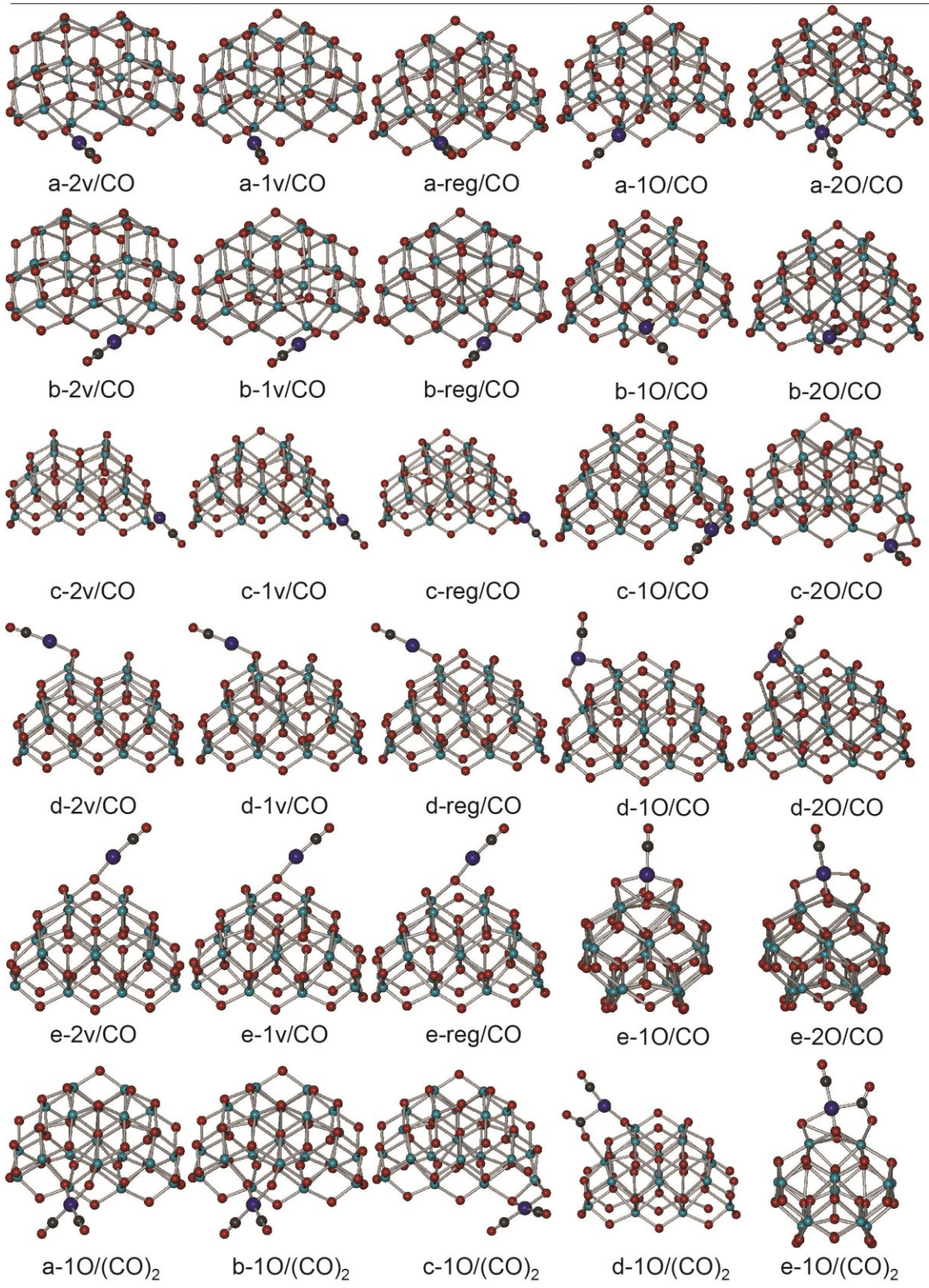

Figure 4

Optimized structures of the complexes $PtO_X(CO)_Z/Ce_{21}O_{42-Y}$ (X, Y = 0 to 2; Z = 1, 2). Five different studied locations of atomic Pt on the surface of the ceria particle are labelled by letters (a)–(e) see Ref. 8 for details. Complexes $Pt/Ce_{21}O_{42}$ in different series are labelled as reg (X = Y = 0), whereas 1O and 2O indicate addition to the reg system of one (X = 1) and two (X = 2) O atoms, and 1v and 2v denote creation in the reg structure of one (Y = 1) and two (Y = 2) O vacancies,respectively. In the five first rows complexes with one CO molecule are presented, while on the bottom row complexes with two CO molecules are presented on $PtO/Ce_{21}O_{42}$ systems. Color coding: red – O; gray – C; light blue – Ce; dark blue – Pt.

Table 3. Energetic and structural characteristics of the $PtO_X(CO)_n/Ce_{21}O_{42-Y}$ (X, Y = 0 ÷ 2, n = 1, 2) complexes. Energy values are in eV, distances in pm, and vibrational frequencies in cm^{-1}.

	Ns[a]	OS(Pt)[b]	BE	E_{rel}[c]	r(Pt-C)	ν(C-O)[d]	Δr(C-O)[e]	r(Pt-O)
a-reg/CO	0	0	-3.57	0.02	182	2032	2.6	200
b-reg/CO	0	0	-3.74	0.01	182	2031	2.6	200
c-reg/CO	0	0	-3.12	**0.00**	183	2010	2.9	196
d-reg/CO	0	0	-3.36	0.25	182	2019	2.8	199
e-reg/CO	0	0	-0.62	0.03	182	2023	2.7	200
a-1V/CO	2	0	-3.94	**0.00**	182	2021	2.9	199
b-1V/CO	2	0	-3.17	0.33	182	2027	2.8	199
c-1V/CO	2	0	-3.39	0.06	182	2002	3.1	195
d-1V/CO	2	0	-3.49	0.51	182	2020	2.8	199
e-1V/CO	2	0	-0.76	0.17	182	2016	2.9	199
a-2V/CO	4	0	-3.10	0.69	182	2022	2.9	199
b-2V/CO	4	0	-3.49	0.67	182	2016	2.8	198
c-2V/CO	4	0	-3.34	**0.00**	182	2001	3.1	196
d-2V/CO	4	0	-3.53	0.55	182	2016	2.9	199
e-2V/CO	4	0	-0.65	0.66	182	2013	2.9	199
a-1O/CO	0	2	-1.88	0.69	187	2042	2.0	191, 198
b-1O/CO[i]	0	2	-1.04	1.93	185	2077	1.5	197, 206, 232
c-1O/CO	0	2	-2.31	0.45	185	2066	1.7	202, 205, 212
d-1O/CO	0	2	-1.90	0.97	186	2046	2.1	189, 200
e-1O/CO	0	2	-1.19	**0.00**	186	2052	1.9	196, 210, 210
a-2O/CO	0	4	-3.02	0.85	188	2095	1.1	187, 190, 200
b-2O/CO[i]	0	2	-2.22	2.40	187	2026	2.2	191, 207, 213
c-2O/CO	0	4	-1.08	1.55	188	2096	1.1	186, 205, 206, 214
d-2O/CO	0	4	-0.40	1.17	198	2121	0.4	185, 193, 193
e-2O/CO	0	2	-2.51	**0.00**	186	2059	1.8	198, 207, 210
a-1O/$(CO)_2$[h]	0	2	-1.98[f]	0.89	189, 190	2074, 2126	0.9, 1.2	196, 201
b-1O/$(CO)_2$[h]	0	2	-2.17[f]	0.91	189, 190	2074, 2125	1.0, 1.1	195, 201
c-1O/$(CO)_2$	0	2	-1.68[f]	1.69	189, 190	2086, 2142	0.6, 1.1	199, 204
d-1O/$(CO)_2$	0	2	-2.54[f]	0.08	184, 220[g]	1861, 2061	2.0, 6.9[g], 10.3[g]	199
e-1O/$(CO)_2$	0	2	-1.74[f]	**0.00**	185, 207[g]	1692, 2074	1.7, 7.6[g], 20.6[g]	202, 225

[a] Number of unpaired electrons; [b] (presumed) oxidation state of Pt; [c] Relative energies with respect to the most stable structure with each stoichiometry; [d] Frequencies are corrected by 14 cm^{-1}; [e] Elongation of C-O bond upon adsorption with respect to the calculated bond length in gas-phase CO of 114.2 pm; [f] BE per CO ligand; [g] Formation of CO_2 is observed; [h] Structures a-1O/$(CO)_2$ and b-1O/$(CO)_2$ are identical; [i] The structures are significantly less stable than the other structures in the corresponding series and will be not considered in the text and figures.

Comparison of the complexes of the same composition shows that four of the complexes $PtCO/Ce_{21}O_{42}$ in series a, b, c and e have essentially equal relative stability (within 0.03 eV), even the fifth structure in series d is only by ~0.20 eV less stable than the others (see Figure 5). This observation suggests that the neutral complex [PtCO] has no particular preference for binding position on the ceria nanoparticle, with BE(PtCO) of -2.24 ÷ -2.49 eV. It is different from the individual platinum atom, which has strong preference for binding in position e. BE(CO) values for the monoatomic Pt^0 species, -3.12 ÷ -3.74 eV, are also higher than the BE values for [PtCO] complex on the ceria particle, which means that Pt-C bond is stronger than Pt-O bond in the $PtCO/Ce_{21}O_{42}$ systems. Hence, we can conclude that [PtCO] species are notably more mobile than the individual Pt species without CO.

The variations in stability of the complexes with different location of the PtCO moiety on the nanoparticle are minor in the complexes with one or two oxygen vacancies (see left-hand part of the solid lines in Figure 5). Under oxidative conditions the stability of the adsorption complexes of CO on PtO_X (X = 1, 2) varies strongly with the position of the complex (Figure 5). The addition of oxygen stabilizes the complex in position e, which becomes the most stable, while complex in position b is strongly destabilized. Note that the relative stability of the different positions for bare Pt species (dashed lines in Figure 5) and PtCO moiety (solid lines in Figure 5) varies differently with oxidation of the platinum species.

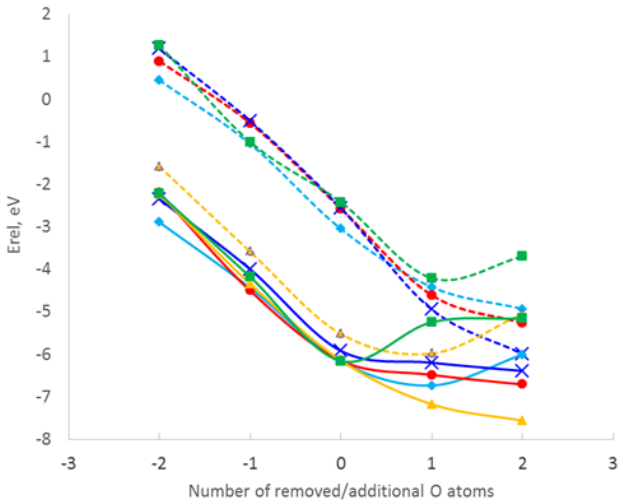

Figure 5. Variation of the relative energy of the modeled complexes with ($PtO_XCO/Ce_{21}O_{42-Y}$, solid lines) and without ($PtO_X/Ce_{21}O_{42-Y}$, dashed lines) CO adsorbed on mononuclear platinum species on ceria nanoparticles as function of the number of removed (-2, -1) or added (1, 2) oxygen atoms. Different series are denoted as a – red circles, b – green squares, c – light blue rhombus, d – dark blue ×, e – yellow triangles.

Complexes with two CO molecules were also investigated for the $PtO/Ce_{21}O_{42}$ structures. In most of the cases (a, b, d and e) BE per CO ligand, -1.74 to -2.54 eV, are higher in magnitude than the corresponding values for the monocarbonyl complexes of Pt^{2+}, similarly to the corresponding isoelectronic complexes of Rh^+ and Ir^+,[50] denoted as complex-specified dicarbonyls.[51-53] In cases d and e one of the CO ligands interacts with the added O atom and CO_2 is formed (Fig. 4). Due to oxidation of CO to CO_2 those structures are more stable than the other considered $PtO(CO)_2/Ce_{21}O_{42}$ complexes (in positions a, b and c) by more than 0.8 eV. Hence, these complexes d and e are promising candidates as precursors of CO oxidation, since the process can be barrierless. During the geometry optimization structures a-1O/$(CO)_2$ and b-1O/$(CO)_2$ became essentially identical.

For CO adsorbed on the stoichiometric $Pt/Ce_{21}O_{42}$ system the C-O vibrational frequencies were calculated to be 2010-2032 cm^{-1}. Formation of one or two O vacancies has a minor effect on C-O frequency, which in general is lowered by ≤10 cm^{-1}. At oxidative conditions, when one O atom is added, platinum species is in oxidation state +2 and the ν(C-O) values, 2043-2066 cm^{-1}, are blue-shifted by about 30 cm^{-1} with respect to the stoichiometric $PtCO/Ce_{21}O_{42}$. When two oxygen atoms are added in the structures a, c and d and Pt is in oxidation state +4, the ν(C-O) values, 2095, 2096 and 2121 cm^{-1}, respectively, are shifted further up, by ~50 cm^{-1}. As described above, in the other two $PtO_2/Ce_{21}O_{42}$ structures the oxidation state of the monoatomic Pt is +2, since O_2^{2-} species are formed and the C-O vibrational frequencies are 2026 and 2059 cm^{-1}. We also modeled a structure where $[PtOPt]^{2+}$ is deposited on ceria nanoparticle. In this case both Pt species are in oxidation state +1 and the calculated frequencies are 2030 and 2042 cm^{-1}, overlapping with the regions of CO on platinum in oxidation states 0 and +2.

The antisymmetric and symmetric C-O frequencies of $Pt^{2+}(CO)_2$ in position e are 2068 and 2117 cm^{-1}, respectively, on $Ce_{21}O_{42}$ support. The corresponding frequencies of the dicarbonyls $PtO(CO)_2$ at different positions on the ceria particle are in the ranges: 2074-2086 (antisymmetric) and 2125-2142 (symmetric) cm^{-1}.

In our previous study[8] we showed that Bader charges on mononuclear Pt species supported on $Ce_{21}O_{42}$ nanoparticle depend on the oxidation state and the coordination of the Pt. We found that Pt charges of -0.08 – 0.11 |e|, 0.62 – 0.69 |e|, 0.85 – 0.90 |e| and ~1.3 – 1.4 |e| correspond to Pt species in the oxidation states 0, +2 (two-coordinated), +2 (three-coordinated), and +4, respectively. In this study we considered the correlation of the calculated C-O vibrational frequency with the oxidation state (Figure S3) and Bader charge of the platinum species (Figure S4). Fig. S3 shows a general trend for increase of the CO frequency with platinum oxidation state, while the values of the Bader charges in Fig. S4 are disperced.

Discussion

Platinum is among the few elements forming non-classical bulk carbonyls, i.e. compounds where platinum is in a cationic state. The stabilization of these species is considered to be due, to a high extent, to the synergism between the σ- and π-bonds between Pt and CO. It is believed that in the carbonyls of Pt^{4+} the back π-bonding is negligible, while it is the dominant bond in the Pt^0-CO species. For the intermediate Pt oxidation states, different balance between the two bonds exists. It is well known than σ-bonding leads to the increase of CO stretching frequency, while it strongly decreases upon formation of back π-bond.[10] As a result, generally the CO frequency is red shifted with the decrease of the Pt oxidation state.[10] The trend is supported by our results for mononuclear platinum species (see Figure S3).

Reactivity of mononuclear platinum species in square-planar position

In previous theoretical and experimental studies,[5,8] it was found that mononuclear platinum species should be preferentially accommodated as Pt^{2+} in square-planar positions on ceria nanoparticles, if such positions are available. Since those species are very stable compared to Pt atoms in other positions (by more than 2.0 eV) they are likely catalytically inactive without a special activation.[54] Our modeling suggests two possible ways of their activation depending on the redox conditions.

Under reductive conditions, the CO adsorption can reduce Pt^{2+} to Pt^0 accompanied by a displacement of the platinum species aside from their square-planar position in ceria, resulting in formation of a stable Pt^0-CO complex at the edge between

{100} and {111} nanofacets. The stability of this $PtCO/Ce_{21}O_{42}$-e complex is essentially the same as of the Pt^0-CO complexes formed in the other positions on ceria nanoparticle. It suggests similar reactivity and easy migration of the neutral moiety Pt(CO) from {100} to {111} facets. The coordination of two CO molecules to the monoatomic platinum species even stronger stabilizes the complex aside from the square-planar position, since the formed dicarbonyl complex is ca. 2.00 eV more stable than the initial Pt/CeO_2-e structure. After completion of the reaction/process and desorption of the gas molecules the Pt species may go back into their most stable square-planar position.

Activation of the cationic Pt species at the {100} facets can also take place under oxidative conditions, where PtO species are formed at low temperatures and high O_2 pressure according to our reported earlier thermodynamic model.[8] The adsorption energy of CO on such PtO species is higher in magnitude than in the $PtCO/Ce_{21}O_{42}$-e complex by 0.57 eV, i.e. the added O atom activates mononuclear platinum species with respect to CO adsorption. Moreover, the $PtO(CO)/Ce_{21}O_{42}$ complex in position e is the most stable among the different locations of PtO species modeled by us. Hence, we suggest that under oxidative conditions and low temperature Pt^{2+} species in square-planar position on the ceria nanoparticle can adsorb CO due to formation of PtO species. In the complexes with the oxidized mononuclear platinum species, $PtO(CO)/Ce_{21}O_{42}$, the CO molecule is in the vicinity of O centers around platinum, which allows the complex to act as precursor species for oxidation of CO to CO_2. Moreover, in the most stable structures, d-$1O(CO)_2$ and e-$1O(CO)_2$ we found spontaneous formation of CO_2 during the geometry optimization of PtO species interacting with two CO molecules, which implies that the barrier for this process might be very low. Similar mechanism with participation of PtO species was proposed for CO oxidation on mononuclear Pt species adsorbed on FeO_x.[55]

Calculated C-O vibrational frequencies on different platinum species

One of the main goals of the present work is to assist in further analysis of the factors, influencing the frequency shift of CO adsorbed on-top on platinum including not only the oxidation state of the platinum centers, but also their specific coordination. First we consider the models shown in Figure 4. There, the vibrational frequency of on-top CO on neutral mononuclear platinum species on stoichiometric or reduced ceria nanoparticles depends on the Pt-O distance to the nearest oxygen center of ceria, at which the platinum atom is anchored (Figure 6). This effect is likely due to increasing polarisation of the electron density between platinum species and the oxygen center when the Pt-O distance increases, which results in an increase of the C-O vibrational frequency.

Our models of unsupported platinum moieties (Pt(111) slab, Pt_{79} and Pt_8 particles) show that coordination number (CN) of the Pt atom to which CO is bound has a significant effect on the C-O vibrational frequencies (Fig. 7). The v(CO) value is 2077 cm^{-1} in our Pt(111) model with CN = 9 and it lowers to 2039-2041 cm^{-1}, when CN = 5, and to even lower frequency 2019-2029 cm^{-1}, when CN = 2 and 3 in the Pt_8 cluster. The flexibility of the Pt surface can also influence the v(CO) values. For instance, v(CO) value of CO adsorbed on the terrace site of {111} facet of Pt_{79}, 2065 cm^{-1}, is by 12 cm^{-1} lower than the corresponding value calculated on the more rigid Pt(111) periodic model, 2077 cm^{-1}. This larger flexibility can be seen, for instance, from the Pt-Pt distances between the Pt atom to which CO is bound and the nearest Pt atoms from the second layer below.

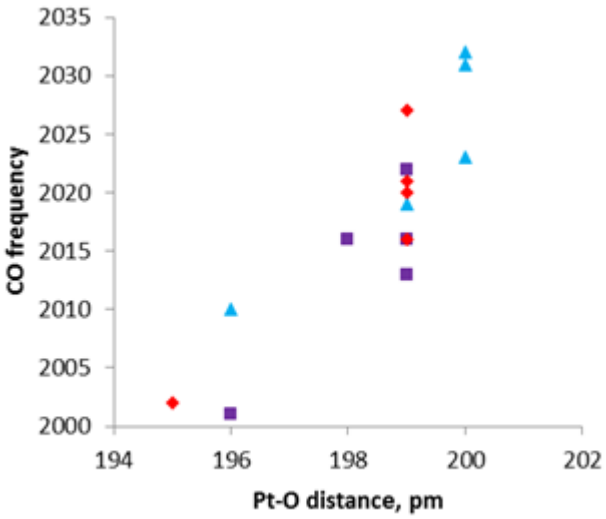

Figure 6. Calculated C-O vibrational frequency for CO adsorption on-top on neutral mononuclear platinum species versus the Pt-O distance (in all structures platinum atom is coordinated to one oxygen center of ceria): violet squares – ceria nanoparticle with two oxygen vacancies, red rhombus – ceria nanoparticle with one oxygen vacancy, blue triangles – stoichiometric ceria particle.

Those distances are: 292, 294, and 294 pm in the more rigid Pt(111) model and significantly more dispersed: 283, 315, and 329 pm in the Pt_{79} nanoparticle. When Pt_8 cluster is supported on ceria nanoparticle, the CO vibrational frequency is lowered by ~20 cm^{-1}. The spillover of one O atom does not noticeably change the C-O vibrational frequency, even when CO is co-adsorbed with an O atom on one Pt atom.

When the probe molecule CO is adsorbed on-top on platinum atom of a neutral isolated platinum cluster, nanoparticle or (111) surface, we observe large variations of the calculated C-O frequency in the range 2000-2080 cm^{-1}. For those species (red rhombus and grey circles in Fig. 7) there is a clear trend to increase the CO frequency with increasing the coordination number of the platinum atom accommodating CO with respect to the other platinum atoms. Those points form a trend line, shown as solid line in Fig. 7, with the equation v = 2003 + 7.11 * CN (with root mean square deviation of 0.89). Analogous correlation, v = 1948 + 16.5 * CN, based on analysis of experimental stretching frequency of CO adsorbed on various platinum-containing samples, was reported in 1991 by Kappers

and van der Maas.[56] They assume specific coordination numbers of the Pt center based on information on the size of the metal moiety and metal dispersion. The difference between the values of the intercept and the slop in the Kappers-van der Maas correlation and our values may originate both from inaccuracies in calculating of the vibrational frequency in our computational approach and in determination of the coordination number of platinum species in the experimental case.

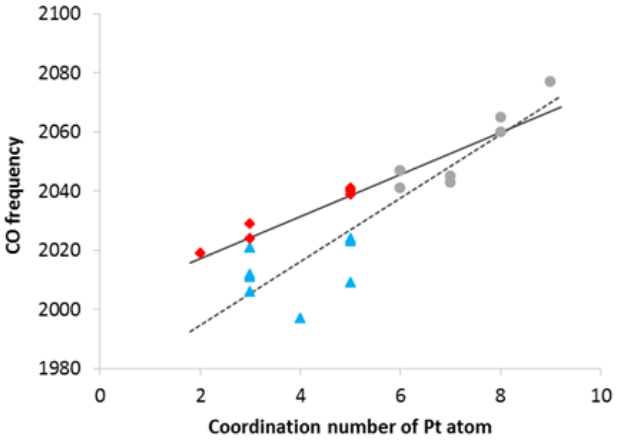

Figure 7. Calculated C-O vibrational frequency for CO coordinated on-top on neutral platinum moeties versus the coordination number of the platinum atom (with respect to other Pt atoms) at which CO is bound: red rhombus – CO at isolated Pt_8 cluster, blue triangles – CO at Pt_8 cluster supported on ceria nanoparticle, grey circles – CO on Pt(111) surface or on the Pt_{79}, Pt_{69}, Pt_{51}, or Pt_{32} nanoparticles. The solid line shows the trend v = 2003 + 7.11 * CN formed by calculated CO stretching frequency and coordination number of the platinum atom in isolated Pt_8 cluster, Pt(111) surface and platinum nanoparticles. The dashed line shows the trend v = 1973 + 10.8 * CN formed by the data for supported Pt_8 cluster instead of isolated one.

The equation for the calculated trend line may approach the experimental one if the dataset instead of values for isolated platinum cluster includes those for supported platinum cluster, v = 1973 + 10.8 * CN (with RMSD = 0.82; dashed line in Fig. 7). This suggests that the experimental trend likely involves both the effects of coordination number of the platinum atom and the effect of the support.

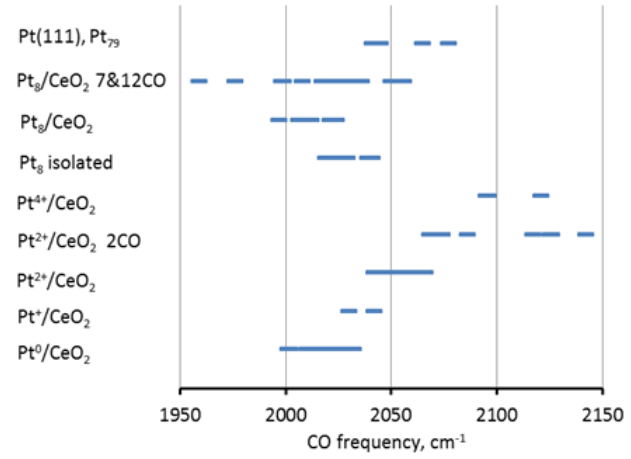

Figure 8. Regions of the calculated C-O vibrational frequency for CO adsorbed on-top of neutral or ionic platinum species from various systems described in the text.

Due to the opposite trends shown in Figure 6 and Figure 7 and the combined influence of neighboring platinum and oxygen centers, we could not identify a clear trend for changes of the vibrational frequency of CO adsorbed on the structures where the metal Pt_8 cluster is supported on ceria nanoparticle (see the blue triangles in Figure 7).

All calculated vibration frequencies of CO adsorbed on-top on various modeled platinum species are shown schematically in Figure 8. The region of the CO frequencies calculated for molecules adsorbed on neutral mononuclear platinum species, 2000 – 2032 cm^{-1}, essentially coincides with the frequency region for CO adsorbed on-top on a platinum atom of isolated or supported Pt_8 cluster, 2019 – 2041 and 1997 – 2024 cm^{-1}, respectively. Adsorption of larger amount of CO, as in the models with 7 or 12 CO molecules on the Pt_8 cluster, results in substantial widening of the region of CO frequencies 1959 – 2062 cm^{-1}, in agreement with broad experimental spectra in this region at high CO coverage.[57,58] On the other hand, the frequencies calculated for the on-top adsorption of CO on Pt(111) surface or on different positions of Pt_{79} nanoparticle, 2041 – 2077 cm^{-1}, overlap to a large extend with the frequencies calculated for monocarbonyls at the mononuclear Pt^{2+} species on ceria nanoparticle, 2042 – 2066 cm^{-1}. Interestingly, the adsorption energies of CO on those two types of platinum centers are also similar (Tables 2 and 3). The C-O frequencies calculated for the molecule adsorbed on mononuclear Pt^{4+} species on ceria nanoparticle, 2095 – 2121 cm^{-1}, are well separated from the frequencies calculated for other monocarbonyl complexes. The upper part of this region, however, overlaps with the symmetric mode of the Pt^{2+} dicarbonyls.

Comparison of the calculated C-O vibrational frequencies with experimental data

As a benchmark of the accuracy of our simulated vibrational C-O frequencies we use the study by Rupprechter et al.,[57] who measured 2081 cm^{-1} for CO adsorbed on top of a platinum atom on the Pt(111) surface at low coverage. This value deviates by only 4 cm^{-1} from the calculated by us v(CO) value for the CO adsorption on Pt(111) surface, 2077 cm^{-1}. The IR band at 2080 cm^{-1}, measured by Happel et al.[22] for Pt/CeO_2 system, was also attributed to CO adsorption on terrace sites of Pt(111) surface of large platinum particles. The band at 2066 cm^{-1} observed by the same authors was assigned to CO adsorbed on the low-coordinated particle edges. However, our calculations suggest that this band may also be due to CO adsorbed on (111) facets of smaller nanoparticles, similar to our model Pt_{79}, with calculated v(CO) of 2065 cm^{-1}. A similar band, 2054 cm^{-1}, was detected by Bazin et al.[4] and was attributed to CO adsorption on terrace sites. Happel et al.[22]

proposed assignment of the band at 2053 cm^{-1} to CO adsorbed close to the interface between Pt and reduced ceria support, CeO_{2-x}. The intensity of this band increases with the amount of the adsorbed CO and it was suggested that adsorption of large amount of CO can lead to reverse electron transfer from ceria support to the platinum moiety. Our calculations corroborate this suggestion – when CO/Pt ratio is close to 1.0 (as in the model with seven or twelve CO molecules adsorbed on Pt_8 supported on ceria) one or two electrons from reduced ceria support are transferred back to the platinum cluster. In addition, in those structures C-O frequencies in the range 2050-2062 cm^{-1} were calculated, together with several bands at lower frequencies. Alternatively, the experimentally detected bands at 2053-2054 cm^{-1} can be assigned to CO adsorption on low coordinated sites of Pt nanoparticles, since our calculations show that CO molecules adsorbed on edges and corners of Pt_{79} have frequencies at 2045 and 2041 cm^{-1}, respectively.

In the study of Bazin et al.,[4] where Pt/CeO_2 samples contained small Pt clusters, two bands were detected at 2033 and 2008-2010 cm^{-1} and attributed to CO adsorption on low and very low coordinated sites of Pt clusters. Our calculations for CO adsorption on platinum atoms in different coordination (from a small particle) are in good agreement with these results: the first band may be assigned to CO adsorbed on platinum atoms with CN = 4-5, while the second one to CO on platinum centers with CN = 2-3. Another reported band at 1937 cm^{-1} was proposed to originate from CO coordinated in a bridge fashion to a platinum and cerium cation or from CO adsorbed on very low coordinated platinum sites.[4] In order to examine the first hypothesis we modeled several structures with the supported Pt_8 cluster, where initially CO was coordinated at the interface, bridging simultaneously one platinum atom and one cerium cation. In all simulations the CO molecule moved to on-top coordination to the platinum center, which does not support the hypothesis. According to our results, the coordination of CO to a very low coordinated platinum site is also unlikely explanation, since the bands for such complexes are predicted by calculations to appear around 2000 cm^{-1}.

Several experimental studies[4,22,23] detected IR bands at 2090-2120 cm^{-1}, which were assigned to the CO adsorption on oxidized platinum clusters or particles, i.e. co-adsorption of CO and O on the same or neighboring platinum atoms. Our data for CO adsorption on mononuclear Pt^{4+} in PtO_2 species supported on ceria nanoparticle, 2095-2121 cm^{-1}, agree well with the experimental results. Hence, we can suggest that this band can be assigned to CO adsorption on Pt^{4+} centers. The vibrations for monocarbonyls of Pt^{2+} were calculated at lower frequencies, around 2042-2066 cm^{-1}, which some authors[23] assigned to adsorption complexes with $Pt^{\delta+}$ (2086-2092 cm^{-1}) or atomic Pt^0 (2066-2085 cm^{-1}) species. For CO adsorbed on samples containing Pt atoms dispersed on a FeO_x support a band at 2080 cm^{-1} was detected and assigned to the adsorption on oxidized monoatomic Pt.[32] Our calculations back up this assignment, if the behavior of FeO_x support is considered similar to that of ceria, where we assign ν(CO) values at 2042-2066 cm^{-1} and 2095-2121 cm^{-1} to CO adsorbed on Pt^{2+} and Pt^{4+}, respectively.

The bands at 1875 cm^{-1} and 1833 cm^{-1} were attributed to bridge CO coordination on platinum.[22,23] Indeed, our calculations for CO adsorbed in bridge positions show ν(CO) values in the range 1840-1885 cm^{-1}, in reasonable agreement with these experimental bands.

Conclusions

Our periodic density functional calculations of a series of platinum containing models help to clarify various experimentally detected bands for CO adsorbed on Pt/CeO_2 samples and give suggestions, where the infra-red bands of CO molecules with certain coordination environment are expected to be found. For instance, bridge CO on Pt is expected to exhibit a band in the region 1840-1885 cm^{-1}. On-top adsorbed CO on metallic Pt^0 should be manifested in the region 2019-2077 cm^{-1}, depending on the coordination number of Pt atoms, from 2 to 9, as the decrease of the coordination number by one lowers the CO frequency by 7.1 cm^{-1}. This theoretical result corroborates the correlation derived by Kappers and van der Maas, from analysis of experimental stretching frequency of CO adsorbed on various platinum-containing samples.[56] The flexibility of the platinum surface also influences the C-O vibrational frequencies, as more flexible surfaces bind CO stronger and shift C-O vibrational frequencies to lower values.

ν(C-O) values for CO adsorbed on stoichiometric mononuclear Pt species supported on ceria are in the range 2010-2032 cm^{-1}. The frequency does not change notably at reductive conditions, when one or two O vacancies are created. However, at oxidative conditions, when one or two O atoms are added to the Pt atom, the C-O vibration is shifted notably to higher frequencies: ν(CO) values are 2042-2066 cm^{-1} and 2095-2121 cm^{-1} for CO adsorption on Pt^{2+} and Pt^{4+}, respectively. Pt^{2+} species form very stable square planar dicarbonyl complexes with frequencies at 2066-2086 cm^{-1} (antisymmetric) and 2115-2142 cm^{-1} (symmetric).

Adsorption of large amount of CO on small Pt clusters can lead to back donation of electrons from ceria support to the Pt cluster; hence, it can reduce the concentration of Ce^{3+} cations. Spillover of one O atom from ceria support to the small Pt clusters does not change notably the binding energy of the CO and its vibrational frequency.

Under reducing conditions the most stable sites for mononuclear Pt species on nanostructured ceria are at small {100} facets. The same sites are the most stable for PtO species, while at strongly oxidative conditions for PtO_2 the most stable positions are sites d at {111} nanofacets of ceria.[8] When CO is adsorbed the preferred adsorption sites are exchanged: under reducing conditions preferred positions of the PtCO complexes are at {111} facets, while at oxidative conditions preferred positions of the PtOCO complexes are at the small {100} facets. Under reducing conditions CO can pull out Pt species from the most stable positions at {100} facets, hence making the Pt species more reactive. At oxidative

conditions Pt species tend to stay at the same position, however oxygen can activate the latter. For instance, the second CO molecule adsorbed on platinum is predicted to be easily oxidized to CO_2.

In summary, comparing the calculated vibrational frequencies of CO in various model systems we concluded that the actual state of the platinum species may be mistaken based only on the measured value of the C-O vibrational frequency due to overlapping regions of frequencies corresponding to different types of species. As often done in the experimental studies, one should follow the changes in the spectra with the amount of CO, temperature, reductive or oxidative pretreatments in order to identify the actual state of platinum species.

Acknowledgements

Support by Bulgarian National Science Fund (Contract DCVP 02/2), Spanish MINECO (grants CTQ2012-34969 and CTQ2015-64618-R, co-funded by FEDER), Generalitat de Catalunya (projects 2014SGR97 and XRQTC), the FP7 program (project FP7-NMP.2012.1.1-1 ChipCAT, Ref. Nº310191 as well as COST Action CM1104), as well as CPU time on BG/P at Bulgarian Supercomputing Center is gratefully acknowledged.

References

1 P. Luches, F. Pagliuca and S. Valeri, *J. Phys. Chem. C*, 2011, **115**, 10718–10726.
2 Y. Lykhach, M. Happel, V. Johanek, T. Skala, F. Kollhoff, N. Tsud, F. Dvorak, K. C. Prince, V. Matolín and J. Libuda, *J. Phys. Chem. C*, 2013, **117**, 12483−12494.
3 R. Kopelent, J. A. van Bokhoven, J. Szlachetko, J. Edebeli, C. Paun, M. Nachtegaal and O. V. Safonova, *Angew. Chem. Int. Ed.*, 2015, **54**, 8728−8731.
4 P. Bazin, O. Saur, J. C. Lavalley, M. Daturi and G. Blanchard, *Phys. Chem. Chem. Phys.*, 2005, **7**, 187–194.
5 A. Bruix, Y. Lykhach, I. Matolínová, A. Neitzel, T. Skála, N. Tsud, M. Vorokhta, V. Stetsovych, K. Ševčíková, J. Mysliveček, R. Fiala, M. Václavů, K. C. Prince, S. Bruyère, V. Potin, F. Illas, V. Matolín, J. Libuda and K. M. Neyman, *Angew. Chem. Int. Ed.*, 2014, **53**, 10525–10530.
6 Y. Lykhach, A. Figueroba, M. Farnesi Camellone, A. Neitzel, T. Skála, F.R. Negreiros, M. Vorokhta, N. Tsud, K.C. Prince, S. Fabris, K.M. Neyman, V. Matolín and J. Libuda, *Phys. Chem. Chem. Phys.*, 2016, **18**, 7672−7679.
7 R. Fiala, A. Figueroba, A. Bruix, M. Václavů, A. Rednyk, I. Khalakhan, M. Vorokhta, J. Lavková, F. Illas, V. Potin, I. Matolínová, K. M. Neyman and V. Matolín, *Appl. Catal. B: Environ.*, 2016, **197**, 262–270.
8 H. A. Aleksandrov, K. M. Neyman and G. N. Vayssilov, *Phys. Chem. Chem. Phys.*, 2015, **17**, 14551–14560.
9 K. Ding, A. Gulec, A. M. Johnson, N. M. Schweitzer, G. D. Stucky, L. D. Marks and P. C. Stair, *Science*, 2015, **350**, 189–192.
10 K. I. Hadjiivanov and G. N. Vayssilov, *Adv. Catal.*, 2002, **47**, 307–511.
11 O. Pozdnyakova, D. Teschner, A. Wootsch, J. Kröhnert, B. Steinhauer, H. Sauer, L. Toth, F. C. Jentoft, A. Knop-Gericke, Z. Paál and R. Schlögl, *J. Catal.*, 2006, **237**, 1–16.
12 T. Tabakova, G. Avgouropoulos, J. Papavasiliou, M. Manzoli, F. Boccuzzi, K. Tenchev, F. Vindigni and T. Ioannides, *Appl. Catal. B: Environ.*, 2011, **101**, 256–265.
13 T. Tabakova, M. Manzoli, D. Paneva, F. Boccuzzi, V. Idakiev and I. Mitov, *Appl. Catal. B: Environ.*, 2011, **101**, 266–274.
14 H. S. Gandhi, G. W. Graham and R. W. McCabe, *J. Catal.*, 2003, **216**, 433–442.
15 J. Kašpar, P. Fornasiero and N. Hickey, *Catal. Today*, 2003, **77**, 419–449.
16 S. D. Senanayake, K. Mudiyanselage, A. Bruix, S. Agnoli, J. Hrbek, D. Stacchiola and J. A. Rodriguez, *J. Phys. Chem. C*, 2014, **118**, 25057–25064.
17 A. Bruix, Y. Lykhach, I. Matolínová, A. Neitzel, T. Skála, N. Tsud, M. Vorokhta, V. Stetsovych, K. Ševčíková, J. Mysliveček, R. Fiala, M. Václavů, K. C. Prince, S. Bruyère, V. Potin, F. Illas, V. Matolín, J. Libuda and K. M. Neyman, *Angew. Chem. Int. Ed.*, 2014, **53**, 10525–10530.
18 G. Preda, A. Migani, K. M. Neyman, S. T. Bromley, F. Illas and G. Pacchioni, *J. Phys. Chem. C*, 2011, **115**, 5817–5822.
19 A. Bruix and K. M. Neyman, *Catal. Lett.* 2016, 10.1007/s10562-016-1799-1.
20 M. Y. Mihaylov, E. Z. Ivanova, H. A. Aleksandrov, P. St. Petkov, G. N. Vayssilov and K. I. Hadjiivanov, *Chem. Commun.*, 2015, **51**, 5668–5671.
21 M. Y. Mihaylov, E. Z. Ivanova, H. A. Aleksandrov, P. St. Petkov, G. N. Vayssilov and K. I. Hadjiivanov, *Appl. Catal. B: Environ.*, 2015, **176–177**, 107–119.
22 M. Happel, J. Mysliveček, V. Johánek, F. Dvořák, O. Stetsovych, Y. Lykhach, V. Matolín and J. Libuda, *J. Catal.*, 2012, **289**, 118–126.
23 J. Ke, W. Zhu, Y. Jiang, R. Si, Y.-J. Wang, S.-C. Li, C. Jin, H. Liu, W.-G. Song, C.-H. Yan and Y.-W. Zhang, *ACS Catal.*, 2015, **5**, 5164−5173.
24 D. W. Daniel, *J. Phys. Chem.*, 1988, **92**, 3891–3899.
25 G. Jacobs, L. Williams, U. Graham, G. A. Thomas, D. E. Sparks and B. H. Davis, *Appl. Catal. A: Gen.*, 2003, **252**, 107–118.
26 P. Pillonel, S. Derrouiche, A. Bourane, F. Gaillard, P. Vernoux and D. Bianchi, *Appl. Catal. A: Gen.*, 2005, **278**, 223–231.
27 G. Jacobs and B. H. Davis, *Appl. Catal. A: Gen.*, 2005, **284**, 31–38.
28 A. Holmgren, B. Andersson and D. Duprez, *Appl. Catal. B: Environ.*, 1999, **22**, 215–230.

29 N. Barrabe, K. Föttinger, A. Dafinov, F. Medina, G. Rupprechter, J. Llorca and J. E. Sueiras, *Appl. Catal. B: Environ.*, 2009, **87**, 84–91.
30 T. Jin, Y. Zhou, G. J. Mains and J. M. White, *J. Phys. Chem.*, 1987, **91**, 5931–5937.
31 M. Hatanaka, N. Takahashi, N. Takahashi, T. Tanabe, Y. Nagai, A. Suda and H. Shinjoh, *J. Catal.*, 2009, **266**, 182–190.
32 B. Qiao, A. Wang, X. Yang, L. F. Allard, Z. Jiang, Y. Cui, J. Liu, J. Li and T. Zhang, *Nat. Chem.*, 2011, 3, 634–641.
33 G. N. Vayssilov, Y. Lykhach, A. Migani, T. Staudt, G. P. Petrova, N. Tsud, T. Skála, A. Bruix, F. Illas, K. C. Prince, V. Matolín, K. M. Neyman and J. Libuda, *Nat. Mater.*, 2011, **10**, 310–315.
34 G. N. Vayssilov, A. Migani and K. Neyman, *J. Phys. Chem. C*, 2011, **115**, 16081–16086.
35 J. P. Perdew, J. A. Chevary, S. H. Vosko, K. A. Jackson, M. R. Pederson, D. J. Singh and C. Fiolhais, *Phys. Rev. B*, 1992, **46**, 6671–6687; ibid. 1993, **48**, 4978–4978.
36 G. Kresse and J. Hafner, *Phys. Rev. B*, 1993, **47**, 558–561.
37 Version VASP.4.9; http://cms.mpi.univie.ac.at/vasp/
38 G. Kresse and D. Joubert, *Phys. Rev. B*, 1999, **59**, 1758–1775.
39 V. I. Anisimov, F. Aryasetiawan and A. I. Lichtenstein, *J. Phys. Condens. Matter*, 1997, **9**, 767–808.
40 S. L. Dudarev, G. A. Botton, S. Y. Savrasov, C. J. Humphreys and A. P. Sutton, *Phys. Rev. B*, 1998, **57**, 1505–1509.
41 C. Loschen, J. Carrasco, K. M. Neyman and F. Illas, *Phys. Rev. B*, 2007, **75**, 035115; erratum *Phys. Rev. B*, 2011, **84**, 199906E.
42 Y. Lykhach, S. M. Kozlov, T. Skála, A. Tovt, V. Stetsovych, N. Tsud, F. Dvořák, V. Johánek, A. Neitzel, J. Mysliveček, S. Fabris, V. Matolín, K. M. Neyman and J. Libuda. *Nat. Mater*., 2016, **15**, 284–288.
43 A. Migani, G. N. Vayssilov, S. T. Bromley, F. Illas and K. M. Neyman, *Chem. Commun.*, 2010, **46**, 5936–5938.
44 A. Migani, G. N. Vayssilov, S. T. Bromley, F. Illas and K. M. Neyman, *J. Mater. Chem.*, 2010, **20**, 10535–10546.
45 A. Bruix, A. Migani, G. N. Vayssilov, K. M. Neyman, J. Libuda and F. Illas, *Phys. Chem. Chem. Phys.*, 2011, **13**, 11384–11392.
46 P. Janthon, S. M. Kozlov, F. Viñes, J. Limtrakul and F. Illas *J. Chem. Theory Comput.*, 2013, **9**, 1631–1640.
47 H. J. Monkhorst and J. D. Pack, *Phys. Rev. B*, 1976, **13**, 5188–5192.
48 A. Hu, K. M. Neyman, M. Staufer, T. Belling, B. C. Gates and N. Rösch, *J. Am. Chem. Soc*., 1999, **121**, 4522–4523.
49 K. Chakarova, M. Mihaylov and K. Hadjiivanov, *Micropor. Mesopor. Mater.* 2005, **81**, 305–312.
50 H. A. Aleksandrov, P. St. Petkov and G. N.Vayssilov, *Energy Environ. Sci.*, 2011, **4**, 1879–1885.
51 E. Ivanova, M. Mihaylov, F. Thibault-Starzyk, M. Daturi and K. Hadjiivanov, *J. Catal.*, 2005, **236**, 168–171.
52 E. Ivanova and K. Hadjiivanov, *Phys. Chem. Chem. Phys.*, 2003, **5**, 655–661.
53 K. Hadjiivanov, E. Ivanova, L. Dimitrov and H. Knözinger, *J. Mol. Struct.*, 2003, **661**, 459–463.
54 Y. Lykhach, A. Figueroba, M. Farnesi Camellone, A. Neitzel, T. Skála, F. R. Negreiros, M. Vorokhta, N. Tsud, K.C. Prince, S. Fabris, K. M. Neyman, V. Matolín and J. Libuda, *Phys. Chem. Chem. Phys*., 2016, **18**, 7672–7679.
55 B. Qiao, A. Wang, X. Yang, L. F. Allard, Z. Jiang, Y. Cui, J. Liu, J. Li and T. Zhang, *Nat. Chem.*, 2011, **3**, 634–641.
56 M. J. Kappers and J. H. van der Maas, *Catal. Lett.*, 1991, **10**, 365–373.
57 G. Rupprechter, T. Dellwig, H. Unterhalt and H.-J. Freund, *J. Phys. Chem. B*, 2001, **105**, 3797–3802.
58 A. Haghofer, P. Sonström, D. Fenske, K. Föttinger, S. Schwarz, J. Bernardi, K. Al-Shamery, M. Bäumer and G. Rupprechter, *Langmuir*, 2010, **26**, 16330–16338.